CHAPTER 5

Studies on adsorptive removal of fluoride and nitrate using CaO@CBC

5.1 INTRODUCTION

Nitrate and fluoride pollution in drinking water is a growing concern worldwide. These pollutants can have significant negative impacts on human health and the environment. NO_3^- in drinking water primarily come from agricultural runoff, particularly from the excessive use of fertilizers and animal waste [83,249]. Similarly, industries including machinery, photovoltaic, food processing, leather production, and paper manufacturing, contribute significantly to NO_3^- pollution in nearby bodies of water [78]. F^- in drinking water can originate from natural sources such as rocks and minerals, as well as human activities like industrial discharges and the use of fluoridated water treatment chemicals [250,251]. Excessive levels of NO_3^- in drinking water can lead to methemoglobinemia, also known as "blue baby syndrome," which impairs the oxygen-carrying capacity of the blood, particularly in infants and potential cancer-causing effects through the formation of nitrosamines [81][82]. It also contributes to eutrophication of water bodies and contamination of groundwater [252]. To address this issue, various organisations, such as United States Environmental Protection Agency (USEPA) and the World Health Organization, have implemented strict regulations and guidelines for NO_3^- levels in drinking water and food products. Currently, the utmost quantity of NO_3^- contamination in potable water is set at 50 mg/ L, but it is recommended to maintain a concentration below 10 mg/ L [81,127]. Long-term exposure to high levels of F^- in drinking water can cause dental fluorosis, skeletal fluorosis, and other health issues such as joint stiffness and thyroid dysfunction [157,240]. To prevent fluorosis, World Health Organization (WHO) have established guidelines for the maximum amount of F^- that is allowed in potable water at 1.5 mg/ L.

Various methods have been used to remove NO_3^- and F^- from water sources, including physical, chemical, and biological approaches [162]. Conventional methods (precipitation-coagulation, membrane-based processes, ion-exchange methods) often come with high costs, inefficiencies,

and the potential for generating toxic byproducts [24,251]. Research in the past decade has highlighted adsorption as a particularly advantageous physical method for dealing with NO_3^- and F^- pollution due to its practical operation and less strict application conditions [253]. There has been extensive research on cost-effective and highly efficient adsorbents for NO_3^- and F^- removal recently. Various types of adsorbents, including natural minerals, industrial wastes, biomass, metal oxides and hydroxides, and carbon-based adsorbents, have been developed and evaluated for their effectiveness in removing NO_3^- and F^- from water [165,254].

The primary objective of this study is to investigate the potential of using electric geyser scaling waste for synthesizing Calcium Oxide as a valuable resource to address F^- and NO_3^- contamination in water. The demand for hot water for domestic use, particularly during winter and in colder climates, remains essential in several countries such as Australia, Canada, China, Europe, Mexico, and the USA. As a result, there is widespread use of electric geysers for water heating. Traditional wood-burning cook-stoves used for water heating contribute to air pollution concerns [255]. The use of electric geysers for water heating has become indispensable. As a result of this process, lime/scale is generated in the electric geysers, and the amount of scaling depends primarily on the quality of the input water. Therefore, using hard water leads to higher scale build-up. Mineral deposition mainly occurs in the form of carbonates and bicarbonates, which presents a major challenge for electric geysers. This includes issues such as corrosion, reduced lifespan of the geysers, blockages, and in extreme cases, explosions that can result in increased power requirements and mechanical and electrical problems. Just a thin 1 mm layer of mineral scale can cause energy consumption to rise by 15%, while a thicker 7 mm layer can lead to a 40% increase in energy usage for electric heaters [256]. Domestic water softening is often considered impractical on a smaller scale due to its cost in many areas, leading it to be generally scrapped off and discarded as waste. This waste material has been consistently disposed of in the nearby soil or land based on observations.

Surprisingly, there is no documented utilization of this waste material in existing literature. Typically, tap water contains calcium (Ca) and magnesium (Mg) salts. However, in our case, calcium salts were found to be the predominant component, as confirmed by XRD analysis. The presence of magnesium, if any, was possibly at extremely low levels that was less than the instrument's detection threshold.

The use of calcium oxide as an adsorbent for the removal of F^- from water has already been established, but it has not been extensively explored for nitrate removal [120]. Calcium oxide used in earlier studies is either synthesized chemically or derived from eggshells and other sources containing calcium [257,258]. Surprisingly, derivation of calcium from scaling waste has not been done before. Use of calcium containing materials in drinking water has some limitations. These limitations include increasing pH, effective removal only at initial F^- concentrations above 10 mg/ L, and inability to reduce F^- concentrations below WHO standards [259]. To further increase calcium oxide's capacity to remove both contaminants and overcome those limitations, we have incorporated calcium oxide with biochar using ball milling method, which has been shown to enhance adsorption properties. In contrast, the calcium oxide (CaO) derived from electric geyser scaling waste (EGWS) overcomes these limitations due to biochar's pH buffering capability, providing a cost-effective, sustainable, and efficient solution for F^- removal from water. This study advances research towards achieving SDG 6 (Clean Water and Sanitation) by exploring a sustainable method for removing nitrate and fluoride contaminants from drinking water. The project utilizes waste electric geyser scaling as a source material for synthesizing calcium oxide, a potential adsorbent for water remediation. This approach contributes to SDG 12 (Responsible Consumption and Production) by repurposing waste materials and developing eco-friendly water treatment technologies. The findings hold promise for providing access to safe and affordable drinking water (SDG 6) while minimizing environmental impact (SDG 12).

Ball milling is a cost-effective and eco-friendly technique that eliminates the need for solvents, enabling the creation of nanocomposites without requiring extra chemicals or intricate processes. The process effectively reduces the particle size of metal oxides, resulting in highly functional nanoparticles with increased surface area and reactivity. This leads to improved adsorption properties. Ball milling can alter biochar by exposing organic groups and enhancing sorption sites, improving its adsorption capacity within nanocomposites. This method also enables the inclusion of various materials into the biochar matrix to tailor nanocomposite properties for specific applications and environmental remediation [260,261].

Through this multifaceted investigation, we aim to contribute valuable insights into sustainable F^- and nitrate treatment technologies using waste-derived materials, with potential implications for environmental remediation and solid waste management.

5.2. METHODOLOGY AND EXPERIMENTAL

5.2.1 Preparation of ball milled EGWS modified biochar

Corn Cob biochar (CBC) was prepared by pyrolyzing Corn cob powder, and its detailed procedure is given in chapter 2 (section 2.3). Collected EGWS was powdered using a mortar and pestle, washed thrice with DI water and then subjected to a 48-h drying process in an oven at 80 °C to eliminate moisture. This powdered EGWS was then subjected to thermal treatment by calcining it at 900 ^oC for 4 h. Next, the sample underwent further grinding to serve as a modifying material for raw biochar. Then this calcinated EGWS named as CaO was used to modify raw biochar via ball milling in order to develop the desired adsorbent. To synthesise this corn cob biochar named as CBC and calcinated EGWS were combined in a ball milling container. Approximately 4 g of biochar and calcinated EGWS in a 1:1 weight ratio was placed in a 500 mL zirconia jar with 100 g of zirconia balls of mixed size (5-12 mm diameter) before being exposed to ball milling. The process of mechanical milling took place in a horizontal

oscillatory ball mill under ambient conditions for a duration of 60 minutes. This milled powder was named as CaO@CBC because after calcination of EGWS it converted to calcium oxide as confirmed by XRD.

5.2.2 Characterization of CaO@CBC

The synthesis of CeO_2/BC and its physical as well as chemical properties were characterized with different characterization tools such as TGA, BET, XRD, FTIR, XPS, and pHzpc measurement.

5.2.3 Fluoride batch adsorption experiments

A set of batch experiments was carried out inside a 250 mL Erlenmeyer flask with 25 mL adsorbate solution to assess the impact of different regulating factors (pH, contact time, and initial concentration and temperature). These adsorption tests took place in regulated conditions at a temperature of 25 °±1 ºC and standard pH maintained at 7 ± 0.3. The impact of solution pH was investigated by adjusting the pH within the range of 2 to 11 for 300 minutes with a dose of 1 gL^{-1} of adsorbent.

Kinetic studies were investigated with distinct initial concentrations of 10, 20, and 30 mg/ L for fluoride and 16, 30 and 40 mg/ L for nitrate, while maintaining a constant adsorbent dosage of 1 gL^{-1} and pH at 7 ± 0.3 for each with continuous shaking for 300 minutes. The samples were subjected to centrifugation, and the remaining fluoride and nitrate concentrations were determined at specified time intervals. Adsorption isotherm studies for both fluoride and nitrate were explored by using solutions with varying concentrations, ranging from 5 mg/ L to 45 mg/ L for fluoride and 10 mg/ L to 50 mg/ L for nitrate at temperatures 293 K, 303 K, and 313 K. Dose of adsorbent, pH and contact time were same as kinetics experiment. The quantification

of remaining fluoride and nitrate ions in the solution was performed using a Metrohm Dual Channel 930 Compact IC Flex.

5.3. BIOCHAR SAMPLE CHARACTERISATION

5.3.1. TGA analysis

The thermal stability of the as-obtained uncalcined Electric Geyser Waste Scale build-up (EGWS) was investigated through Thermogravimetric Analysis (TGA). The TGA plot, illustrated in Figure. 5.1a, delineates the relationship between weight loss and temperature. The TGA profile of EGWS reveals two distinct stages of weight loss. The initial stage, accounting for a weight loss of 3.06%, occurs up to a temperature of 600 °C. The extent of weight lost during this temperature is due to the extraction of water molecules from the EGWS, commonly referred to as dihydroxylation with the release of carbon dioxide CO_2. The second stage of weight loss, i.e., 40.05 % observed between 600 °C and 791 °C. The primary decomposition of EGWS into calcium oxide (CaO) and carbon dioxide (CO_2) transpires in the temperature range (600 to ~800 °C). The reaction involves the breakdown of bonds within the EGWS due to applied heat, resulting in the formation of calcium oxide and the release of carbon dioxide gas. The decomposition of EGWS is complete as indicated by the stable mass of the material after reaching a temperature of 800 °C.

5.3.2 XRD analysis

XRD diffractograms of raw EGWS, synthesised calcium oxide through EGWS by calcining at temperature 900 ºC, unmodified biochar and biochar modified by CaO derived from EGWS through ball milling are presented in Figure. 5.1b. They are respectively named EGWS, CaO, CBC and CaO@CBC. From the Figure 5.1b, it can be seen that the XRD diffractograms of the raw EGWS, synthesised calcium oxide through EGWS, unmodified biochar, and biochar modified by CaO all exhibit distinct diffraction patterns except CBC. The diffraction peaks

observed in CBC in the *2θ* range of 20 ° to 30 ° align with the stacking arrangement of graphite's aromatic layers (graphite 002).

Analysis of the XRD diffractograms reveals the presence of $CaCO_3$ in orthorhombic aragonite form (JCPDS file no. 05-0453) in raw EGWS. Upon calcination, the carbonate peaks transform into the cubic CaO phase, evident by peaks at *2θ* values of 34.06, 54.34, 62.46, 64.22, and 79.15 (JCPDS File No. 37-1497). Additionally, larger and less defined peaks at *2θ* equals to 17.94, 28.5, 46.57, 50.80, and 71.76, characteristic of Ca $(OH)_2$, are present, indicating the reaction of CaO with ambient moisture. These XRD results provide clear evidence of the transformation of EGWS into calcium oxide through the process of calcination.

5.3.3 BET analysis

BET analysis was conducted of all the synthesised adsorbents to evaluate the surface area and porosity of raw Corn Cob biochar (CBC), CaO, and CaO@CBC, revealing isotherms consistent with type IV patterns featuring an H2 hysteresis loop (Figure. 5.1c) (Table 5.1). This behaviour suggests the mesoporous nature of the materials, indicating pore sizes ranging between 2 and 50 nm. The BET surface area of CaO derived from Electric Geyser Waste Scale (EGWS) was determined to be 6.02 m^2g^{-1}. Upon ball milling with corncob biochar, possessing a high surface area of 228.08 m^2g^{-1}, the surface area substantially increased to 78.31 m^2g^{-1}. This augmentation is attributed to the robust interaction between CaO and the biochar support, mitigating surface diffusion of calcium and stabilising the CaO surface [262]. This increase in surface area of synthesised CaO from EGWS also proves that ball milling has helped in increasing the surface area [260] .

The modified CaO, denoted as CaO@CBC, is thought to enhance the adsorption process by making active sites accessibility and providing ample attachment areas, as previously reported by Istadi et al. (2015) [263]. The total pore volume and average pore diameter of CaO, biochar (CBC), and CaO@CBC were determined as 0.05 cm^3g^{-1} and 33.48 nm, 0.15 cm^3g^{-1} and 2.70

nm, and 0.15 cm^3g^{-1} and 7.94 nm, respectively. Ball milling has also helped in increasing average pore diameter of CaO@CBC as compared to raw biochar [260]. The ball-milled CaO@CBC,s larger average pore diameter and interlinked pores are reported to minimise diffusion limitations for adsorbate molecules, facilitating easy infiltration into the adsorbent's interior. This characteristic ensures the effective utilisation of active sites during the adsorption process [264].

Table 5.1: Comparing values of surface area, pore volume and pore size of synthesised CaO, Corn Cob biochar and modified biochar with CaO@CBC

Sample description	BET surface area (m^2g^{-1})	BJH average pore size (nm)	BJH pore volume (cm^3g^{-1})
CaO	6.02	33.48	0.05
Corn Cob biochar	228.08	2.70	0.15
CaO@CBC	78.31	7.94	0.15

5.3.4 FTIR analysis

FTIR analysis was performed to study the surface functional groups of synthesised adsorbents, as illustrated in Figure. 5.1d. Prior to the adsorption process, distinctive adsorption peaks were evident at 3648, 3428, 1476, 1106, and 869 cm^{-1} among EGWS derived CaO and CaO@CBC. Notably, the sharp peak at 3648 cm^{-1} and the broad peak at 3428 cm^{-1} were attributed to the stretching vibrations of OH originating from Ca $(OH)_2$ and captured water molecules on the surface of the adsorbent, respectively [265]. Peak observed at 1476 and 1106 cm^{-1} were associated with the bending vibrations of C-H and stretching vibrations of C–O bonds [266] in

CaO@CBC. This could be attributed to the bending mode of aromatic compounds present in the biochar. This observation confirms the successful modification of Corn Cob biochar using synthesised CaO. At 871 cm^{-1}, sharp bands related to the Ca–O bond were identified, while broad peaks around 500 cm^{-1} originated from the Ca=O bonds [267].

Following the adsorption process, notable changes were observed. The disappearance of the –OH bond peak at 3648 cm^{-1} in CaO@CBC indicated the interaction of the active Ca–OH site on the surface with F^- and nitrate both. Moreover, the weakening of the Ca–O bond peak at 869 cm^{-1} and the disappearance of the Ca=O bond peaks suggested a reaction between Ca, F^- and NO_3^- during adsorption [268,269]. The strong appearance of N-O peak in CaO@CBC post nitrate adsorption proves that nitrate is successfully removed from water. This transformation in the CaO@CBC spectrum before and after adsorption reaffirms the pivotal role of $Ca(OH)_2$ in F^- and nitrate adsorption. Detailed explanation of post adsorption changes in CaO@CBC are explained in mechanism section.

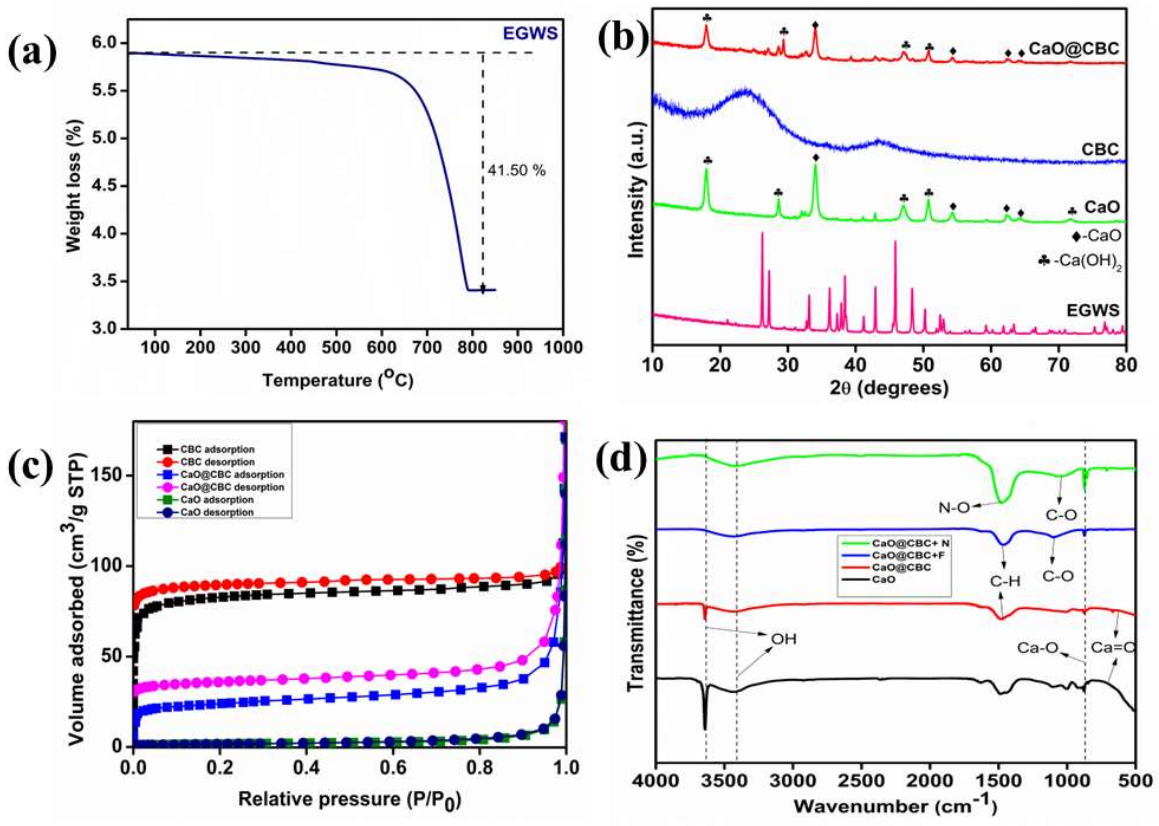

Figure. 5.1 (a) TGA plot of raw Electric geyser waste scale (EGWS); (b) XRD diffractograms of raw EGWS, synthesised CaO at 900 °C, unmodified Corn Cob biochar (CBC) and modified biochar (CaO@CBC); (c) N_2 adsorption-desorption isotherms; (d) FT-IR spectrum of adsorbents before and after adsorption

5.3.5 SEM analysis

The surface morphology of CBC, CaO and CaO@CBC (before adsorption) were analysed using SEM as shown in Figure. 5.2. The SEM image of CBC (Figure. 5.2 a-b) explains that the original xylem existing in the corn cob cell structure remains present after pyrolysis also [193]. As depicted in Figure. 5.2 c-d, the surface of calcium oxide exhibits a distinctive granular structure characterised by well-defined, agglomerated particles. The particles appear to be spherical in shape, with some larger aggregates indicating possible agglomeration during the

synthesis process. The surface texture appears relatively smooth. The SEM analysis of calcium oxide-impregnated biochar (CaO@CBC) unveils a distinct alteration in surface morphology compared to unmodified biochar (CBC). Figure. 5.2 e-f showcases the surface characteristics of CaO@CBC, revealing a heterogeneous structure marked by the presence of irregularly shaped particles. The integration of calcium oxide is evident through the appearance of additional agglomerates and blocking of pores, contributing to a more complex and textured surface. The modified biochar exhibits a combination of the original biochar matrix (honeycomb like structures) and the introduced calcium oxide, indicating an interlink between the two materials. Notably, the interaction between calcium oxide particles and the biochar matrix is observed, suggesting successful impregnation.

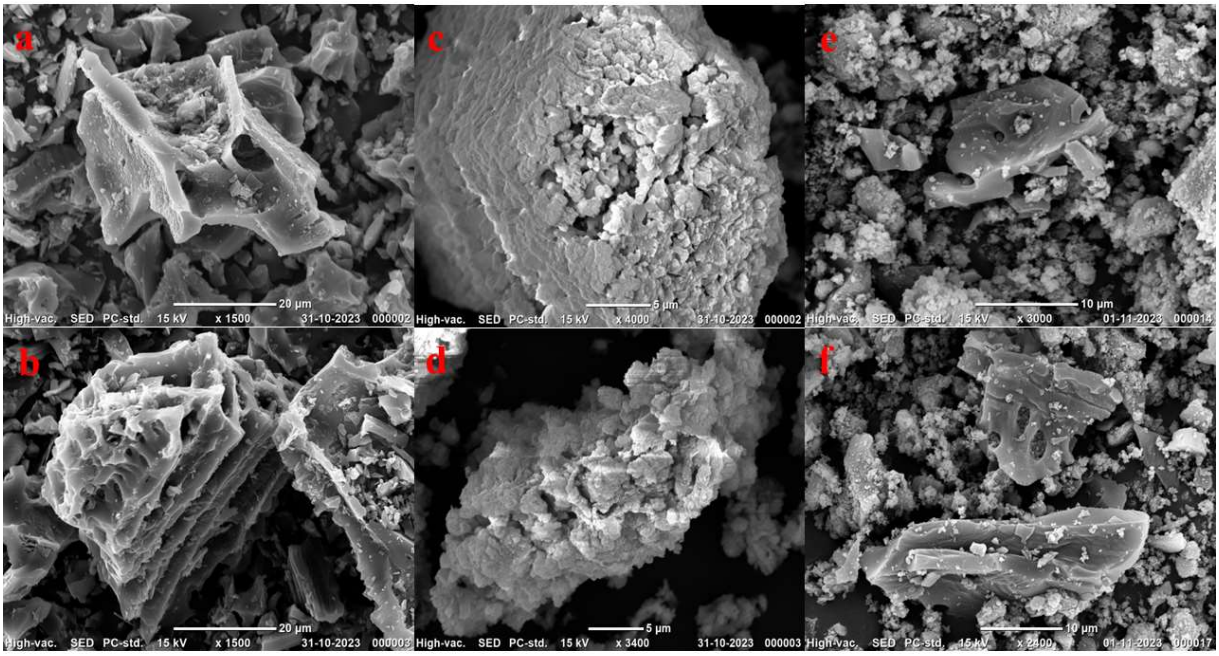

Figure. 5.2: (a and b) SEM images of unmodified Corn Cob biochar, (c and d) synthesised CaO at 900 °C before adsorption; (e and f) CaO@CBC before adsorption

5.4 BATCH ADSORPTION STUDIES

5.4.1 Influence of pH and pHpzc results

The investigation focused on assessing the impact of initial pH on the efficacy of F^- and NO_3^- removal by CaO@CBC. Given that the surface charge plays an essential role in anion adsorption, the Zero Point of Charge (pHpzc) of CaO@CBC was scrutinised under varying pH conditions (ranging from 2 to 12) utilising the Salt Addition Method (Figure. 5.3b). Notably, the surface carries positive charges below pH 10, transitioning to negative charges as the pH reaches 12. The determined pHpzc for CaO@CBC is 10.4. Despite the pH change, CaO@CBC exhibited sustained high adsorption capacities for NO_3^- and F^- across the broad pH range of 4–10 (Figure. 5.3a). NO_3^- removal steadily remained around 60%, while F^- removal remained approximately at 73% within the pH range of 4-8. Remarkably, both NO_3^- and F^- still maintained approximately 50% adsorption at pH levels 9-11. Below a pH of 4, the F^- removal capacity weakened considerably, potentially linked to the forming of hydrofluoric acid, resulting in a notable decrease in F^- availability [203]. Similarly, under highly acidic conditions, protonation of NO_3^- induces a significant reduction in electrostatic attraction between the positively charged adsorbent and protonated NO_3^- ions (HNO_3) [270]. The consistent high removal of NO_3^- and F^- by CaO@CBC aligns with electrostatic adsorption principles and the point of zero charge at pH 10.4.

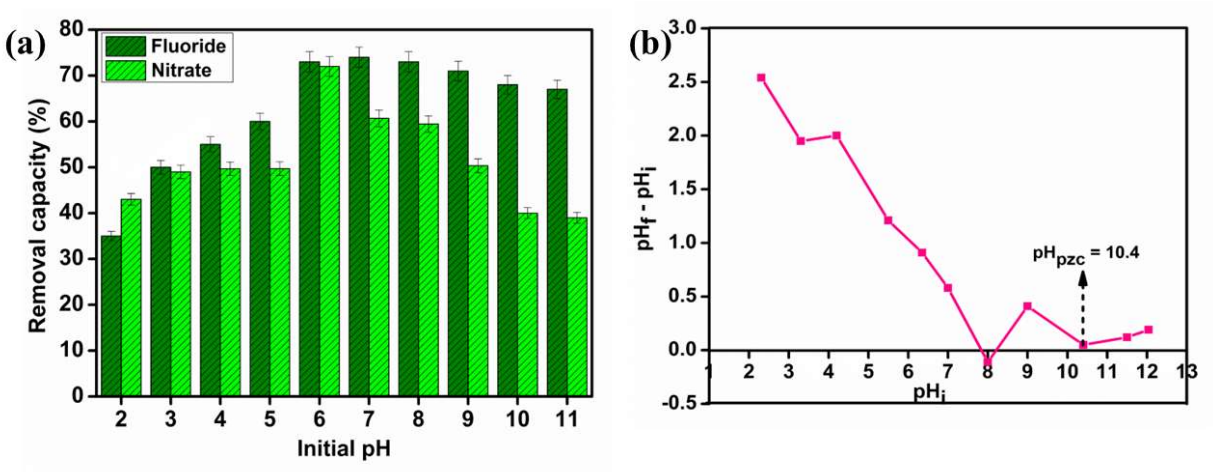

Figure. 5.3 (a) Effect of initial pH on fluoride and nitrate removal percentage of CaO@CBC; (b) pHpzc results of CaO@CBC

5.4.2 Effect of contact time on adsorption and kinetic studies

The effect of contact time on the removal of F^- and NO_3^- by CaO@CBC was systematically investigated to comprehend the kinetics of the adsorption process (Figure. 5.4 a-d). For F^- removal, experiments were conducted with initial concentrations of 10, 20, and 30 mg/ L. At a concentration of 10 mg/ L, a rapid removal of 62% was achieved within the first 30 minutes, reaching equilibrium around 240 minutes with a final removal efficiency of 74% at 300 min. However, at higher concentrations of 20 mg/ L and 30 mg/ L, the adsorption process showed a slower rate, with only 33% removal for 20 mg/ L and 55% for 30 mg/ L at 300 min. Equilibrium was attained over a longer duration, signifying that the adsorption of F^- by CaO@CBC is concentration-dependent, with higher concentrations requiring extended contact time for optimal removal. Similarly, for nitrate removal, experiments were conducted with initial concentrations of 16, 30, and 40 mg/ L. The results revealed a swift removal process, with maximum removal efficiencies of 61%, 67%, and 76% achieved within the first 30 minutes for 16 mg/ L, 30 mg/ L, and 40 mg/ L, respectively. Subsequently, the removal rate slowed down,

reaching equilibrium around 180 minutes, with final removal efficiencies of 72%, 74%, and 78% for 16 mg/ L, 30 mg/ L, and 40 mg/ L, respectively. This indicates that the adsorption of nitrate by CaO@CBC is efficient in the initial stages, and the system approaches equilibrium with prolonged contact time. The kinetic behaviour of F^- and NO_3^- removal using CaO@CBC were further investigated by fitting experimental findings with Pseudo-First order (PFO) (Figure. 5.4 c-f), Pseudo-Second order (PSO) mathematical models (Figure. 5.4 b-e) revealing that both ions follow PSO model with high correlation coefficients (R^2) close to 0.99 in each case [271]. Chapter 2 Section 2.5.2 provides a brief mathematical representation of these models. The high R^2 values suggest a strong agreement between the experimental and calculated data (Table 5.2), showing that the PSO model accurately describes the adsorption process. This model explains the mechanism of CaO@CBC removal of F^- and nitrate by stating that the rate-limiting step is chemisorption, which involves valence forces through electron sharing or exchange.

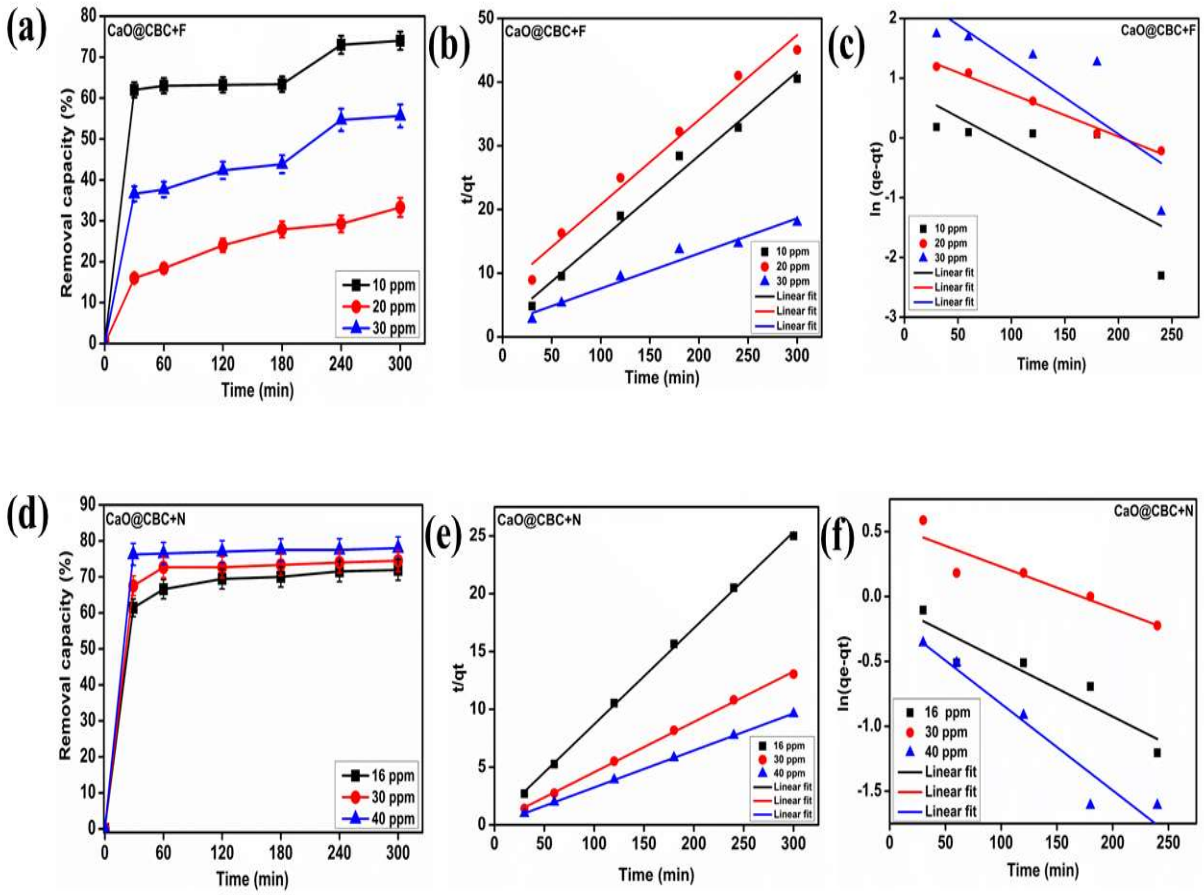

Figure. 5.4 Effect of contact time on fluoride removal (a) and nitrate removal (d); Plots of Pseudo-second-order kinetic model (b and e) for fluoride and nitrate respectively; Plots of Pseudo-first -order kinetic model (c and f) for Fluoride and nitrate respectively

Table 5.2: Different kinetic models' parameter for Fluoride and Nitrate uptake by CaO@CBC

C_0 (mg/ L)	q_e(exp) (mgg^{-1})	Pseudo-first-order			Pseudo-second-order		
		K_1 (min^{-1})	q_e (Cal) (mgg^{-1})	R^2	K_2 (mg min^{-1})	q_e (Cal) (mgg^{-1})	R^2
		Fluoride					
10	7.4	0.00003	2.29	0.45	27.23	7.59	0.98
20	6.656	0	4.27	0.98	7.56	7.514	0.97
30	16.692	0.00004	12.19	0.60	157.55	18.15	0.96
		K_1 (min^{-1})	q_e (Cal) (mgg^{-1})	R^2	K_2 (mg min^{-1})	q_e (Cal) (mgg^{-1})	R^2
		Nitrate					
16	12	0	0.94	0.83	375.85	12.02	0.99
30	23	0	1.74	0.81	2600.83	22.96	0.99
40	31.2	0	0.85	0.91	23766.43	31.25	0.99

5.4.3. Effect of concentration, isotherm and thermodynamic studies

The adsorption isotherms for F^- and NO_3^- on CaO@CBC were thoroughly analysed using Langmuir and Freundlich models, providing valuable insights into the adsorption process efficiency and mechanism. The experiments covered a temperature range of 293 K, 303 K, and 313 K, using NO_3^- concentrations of 10, 20, 30, 40 and 50 mg/ L along with F^- concentrations ranging from 5 mg/ L to 45 mg/ L. The exposure duration for both was 300 minutes (Figure. 4.5 a-d). The adsorption behaviour is indicated by the observed increase in adsorption capacity with an increase in the initial concentration for both F^- and NO_3^-. At lower concentrations, the heightened availability of F^- and NO_3^- ions and increased vacant adsorption sites on the CaO@CBC surface facilitate enhanced adsorption. With rising concentration, a greater number

of F^- and NO_3^- ions interact with the CaO@CBC surface, occupying more sites and resulting in increased adsorption capacity. The experimental findings fitted to Langmuir and Freundlich [153] were compared, as shown in Figure. 5.5 and Table 5.3. Chapter 2 Section 2.5.3 provides a brief mathematical representation of these models. In the case of nitrate and F^- adsorption on CaO@CBC, the Langmuir model demonstrated an excellent fit, with R^2 values exceeding 0.98 for both (Figure. 5.5 b-e). Based on the results obtained from various experiments and models, it is evident that the elimination of F^- and nitrate by CaO@CBC is primarily controlled by monolayer adsorption. It indicates that adsorption is occurring uniformly on the adsorbent surface, with no interaction between adsorbed molecules. The monolayer formation suggests saturation of adsorption sites. This model relies on the assumption of a uniform energy distribution among adsorption sites.

The Langmuir maximum adsorption capacity of CaO@CBC at 303 K for F^- was determined to be 18.36 mg/g, while at 293 K for nitrate, it was 19.27 mg/g. Notably, these values surpass the capacities reported for modified biochar in previous studies for nitrate and F^- adsorption (Table 5.4).

Further investigation into the thermodynamics of adsorption was conducted to comprehend the spontaneity, feasibility, heat changes, and entropy changes occurred with the uptake reactions of nitrate and F^- by CaO@CBC and the values are represented in Table 5.5. All the mathematical equations are given in Chapter 2 section 2.5.4.

The negative $\Delta G°$ values at all temperatures indicate that the F^- and NO_3^- uptake reactions by CaO@CBC are spontaneous and thermodynamically favourable. The negative value of the standard Gibbs free energy change $(\Delta G°)$ for the adsorption process indicates that the nitrate and F^- uptake reactions by CaO@CBC are thermodynamically favourable. This suggests that adsorption of nitrate and F^- onto the CaO@CBC surface is feasible. The $\Delta H°$ and $\Delta S°$ values were calculated as theoretical parameters during fitting processes with the Van't Hoff equation,

while positive signs of $\Delta S°$ point to an increase in randomness properties of these uptake reactions at higher temperatures. The negative $\Delta G°$ values, together with the estimated $\Delta H°$ values, indicate that the nitrate and F^- uptake reactions by CaO@CBC are both spontaneous and exothermic.

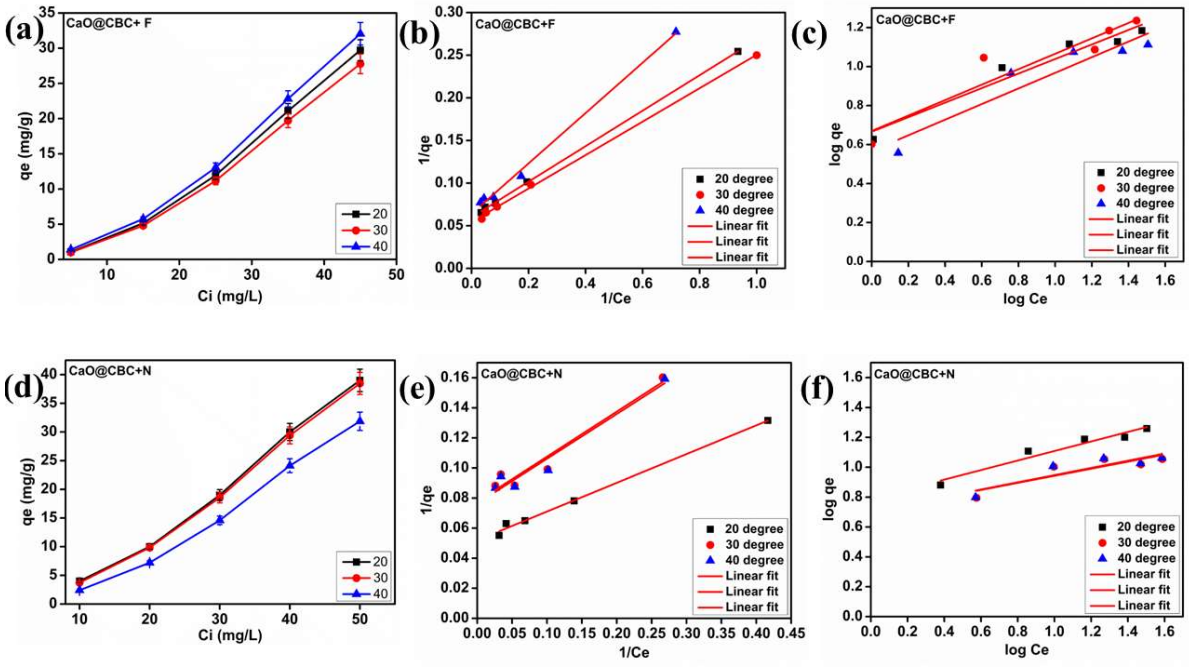

Figure. 5.5 Effect of initial concentration on fluoride removal (a) and nitrate removal (d); Plots of Langmuir isotherm model (b and e) for fluoride and nitrate respectively; Plots of Freundlich isotherm model (c and f) for F^- and nitrate respectively

Table 5.3: Different values of adsorption Isotherms for Fluoride and Nitrate adsorption on CaO@CBC

Isotherm Parameters			**293 K**	**303 K**	**313 K**
Langmuir	Fluoride	Q_0 (mgg^{-1})	16.64	18.36	15.6
		b	79.96	93.65	6.79
		R^2	0.99	0.99	0.99
	Nitrate	Q_0 (mgg^{-1})	12.88	13.09	19.27
		b	100.77	43.03	44
		R^2	0.98	0.93	0.94
Freundlich	Fluoride	K_f (mgg^{-1})	4.63	4.67	3.69
		1/n	0.37	0.39	0.4
		R^2	0.93	0.85	0.85
	Nitrate	K_f (mgg^{-1})	6.16	5.07	5.08
		1/n	0.31	0.23	0.24
		R^2	0.93	0.71	0.72

Table 5.4: Overview of adsorbents utilised in Fluoride and Nitrate removal processes, highlighting their Adsorption Capacities

S.No.	Adsorbent	Adsorbate	Adsorption capacity (mgg^{-1})	pH	Time (min)	References
1	α-Fe_2O_3 and Fe_3O_4 dispersed on Douglas fir biochar	Fluoride	9	7	5	[272]
2	Corn stover biochar	Fluoride	6.42	2	60	[35]
3	Magnetic corn stover biochar	Fluoride	4.11	2	60	[35]
4	Al modified Eucalyptus wood biochar	Fluoride	1.6	6	1440	[211]
5	CaO@CBC	Fluoride	18.36	7	300	This work
6	α-Fe_2O_3 and Fe_3O4 dispersed on Douglas fir biochar	Nitrate	15.53	7	10	[272]
7	$FeCl_3$- impregnated biochar	Nitrate	14	not known	720	[273]
8	CaO@CBC	Nitrate	19.27	7	300	This work

Table 5.5: Theoretical values of thermodynamic parameters for fluoride and nitrate adsorption by CaO@CBC

	Temperature (K)	$\Delta G°$ ($kJmol^{-1}$)	$\Delta H°$ ($kJmol^{-1}$)	$\Delta S°$ ($kJmol^{-1}$ K)
Fluoride	293	-3.17	-13.05	32.98
	303	-3.49		
	313	-2.48		
Nitrate	293	-2.81		
	303	-1.27		
	313	-1.36	-24.5	74.85

5.5 ADSORPTION MECHANISM

It was essential to assess the adsorption mechanism in order to comprehend the characteristics of CaO@CBC and its role in removal of both ions. Results of FTIR analysis post adsorption of F^- and nitrate (Figure. 5.1d) clearly indicates the participation of –OH groups in removing F^- and NO_3^- both indicating that ion exchange could be involved in removal. The weakening of the Ca–O bond peak at 869 cm^{-1} and disappearance of Ca=O bond at 500 cm^{-1} shows that calcium could also be involved in inner–sphere mechanism of adsorption.

The XPS spectra were utilised to examine the qualitative and quantitative molecular-level details of the F^- adsorption mechanism, as depicted in (Figure 5.6 a). Based on the findings from the XPS spectra, it can be observed that after F^- adsorption, the shapes of the Ca 2p peak shapes exhibited a positive shift in binding energy values of 0.3 eV after the adsorption of F^- (Figure. 4.6 a), indicating the replacement of –OH group by the highly electronegative F^- ion [258]. Besides that, the binding energy of F 1s at 684.6 eV was higher than that of NaF peak at 684.5 eV (Figure. 4.6 c). Furthermore, in Figure. 6b, the deconvolution of the O 1s peak identified two chemical states. The O-H peak, situated within an environment possibly containing C-OH and Ca-OH, exhibited a significant positive shift of 0.5 eV after adsorption. This shift suggests the participation of hydroxyl groups and potentially the ion exchange of OH- with $F^{-.}$ The presence of a peak at 532.8 eV also suggests the possible formation of calcium fluoride [274].

Similarly, after nitrate adsorption there is shifting of binding energy y in Ca 2p peak by 0.6 eV which can be due to involvement of OH in complexation reaction (Figure. 5.6 a). In deconvolution peak of N 1 s spectra there is peak at 399.9 eV binding energy indicative of the formation OH calcium nitrate on the adsorbent (Figure. 5.6 d). In O1s spectra there is shift of binding energy after adsorption in O-H peak (at binding energy 531.6 eV) which can be due to

ion exchange process (Figure. 5.6 b). Peak at 533 eV of O1s spectra shows that some nitrate could also be present in form of nitrides bonded with calcium.

From pHpzc results it is evident that surface charge of adsorbent also plays crucial role in adsorption of both ions (Figure. 5.3b). The CaO@CBC exhibited a pHpzc of 10.4, indicating a positively charged surface at lower pH levels (< 10.4) due to protonation of hydroxyl groups bonded to Calcium on its surface. This facilitates the adsorption process for F^- and nitrate ions through protonation/deprotonation of hydroxyl functional groups, leading to electrostatic attraction and formation of bound ion pairs with the positively charged surface.

The chemical equation for the F^- and nitrate adsorption process on CaO@CBC is as follows:

$$Ca\text{-}OH + F^- \rightleftharpoons Ca\text{-}F + OH^- \quad (1)$$

$$Ca\text{-}OH + NO_3^- \rightleftharpoons Ca\text{-}NO_3 + OH^- \quad (2)$$

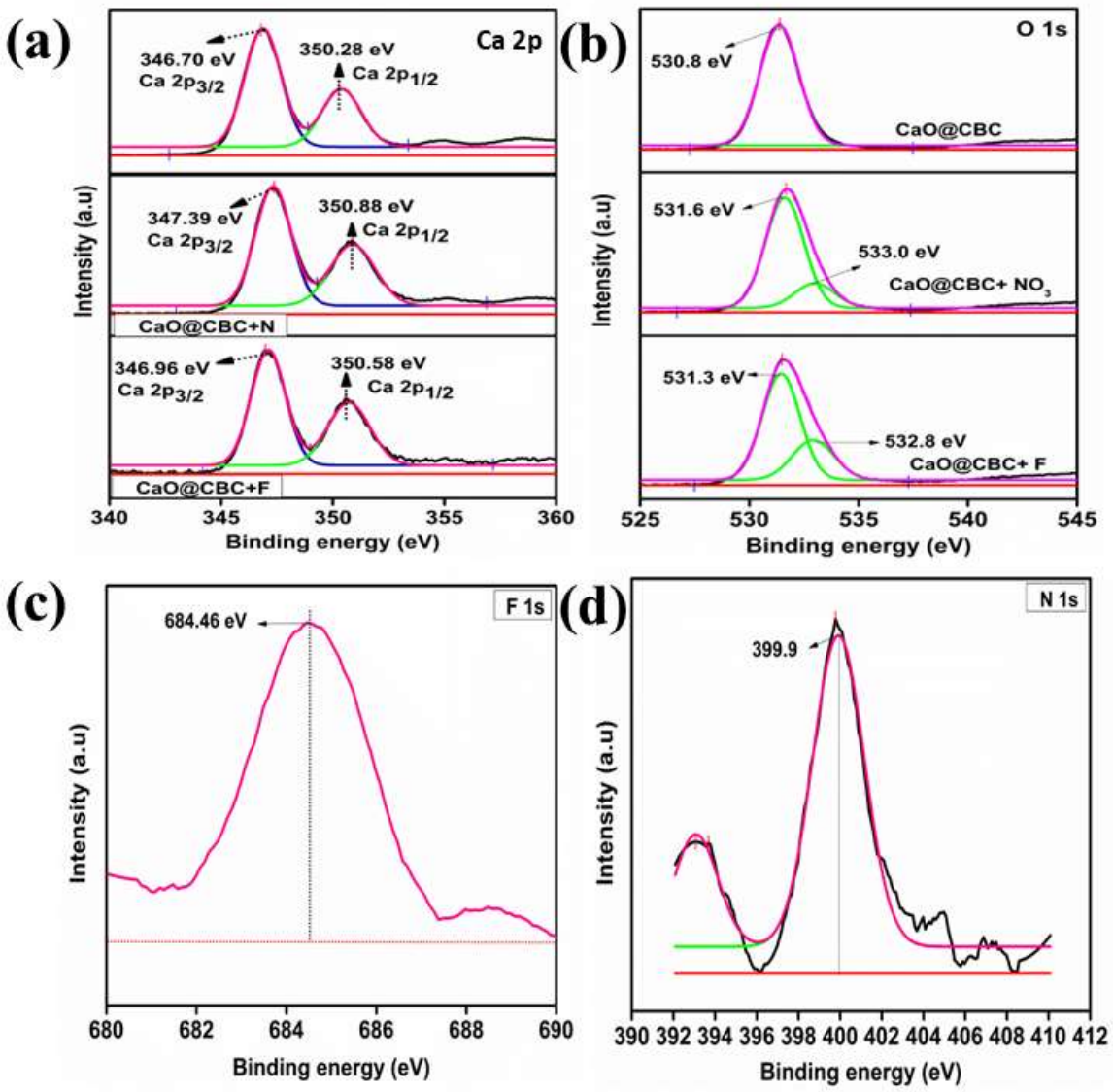

Figure. 5.6 XPS analysis results (a) Ca 2p spectra comparing before and after adsorption changes in CaO@CBC; (b) O 1s spectra; (c) F 1s spectra; (d) N 1s spectra before and after adsorption

5.6 CONCLUSIONS

The study demonstrates the potential of utilising waste material deposition from electric geysers specifically scaling waste as a cost-effective and sustainable resource for biochar modification to remove nitrate and F^-. The modified biochar, produced through ball milling with calcium oxide extracted from the electric geyser waste scale (CaO@CBC), demonstrated remarkable adsorption capacities for both contaminants. The adsorption capacity of CaO@CBC was sustained across the pH range of 2-11. The Langmuir isotherm model fitting suggests a monolayer adsorption mechanism with maximum adsorption capacities of 18.36, 19.27 mgg^{-1} for F^- and NO_3^- respectively. The thermodynamic study of the nitrate and F- uptake reactions by CaO@CBC reveals that the adsorption processes are spontaneous, favourable, and exothermic. The synthesised CaO@CBC exhibited a high surface area and porosity, contributing to its enhanced adsorption efficiency. The findings propose CaO@CBC as a promising, environmentally sustainable adsorbent aligned with circular economy principles, demonstrating electrostatic attraction and ion exchange processes in its adsorption mechanism.